Fully Integrated Point-of-Care Platform for the Self-Monitoring of Phenylalanine in Finger-Prick Blood

Maria Anna Messina, Ludovica Maugeri, Guido Spoto, Riccardo Puccio, Martino Ruggieri, and Salvatore Petralia*

Cite This: https://doi.org/10.1021/acssensors.3c01384

Read Online

ACCESS | Metrics & More | Article Recommendations | Supporting Information

ABSTRACT: Development of point-of-care platforms combining reliability and ease of use is a challenge for the evolution of sensing in healthcare technologies. Here, we report the development and testing of a fully integrated enzymatic colorimetric assay for the sensing of phenylalanine in blood samples from phenylketonuria patients. The platform works with a customized mobile app for data acquisition and visualization and comprises an electronic system and a disposable sensor. The sensing approach is based on specific enzymatic phenylalanine recognition, and the optical transduction method is based on in situ gold nanostructure formation. The phenylketonuria (PKU) smart sensor platform is conceived to perform self-monitoring on phenylalanine levels and real-time therapy tuning, thanks to the direct connection with clinicians. Validation of the technologies with a population of patients affected by PKU, together with the concurrent validation of the platform through centralized laboratories, has confirmed the good analytical performances in terms of sensitivity and specificity, robustness, and utility for phenylalanine sensing. The self-monitoring of phenylalanine for the daily identification of abnormal health conditions could facilitate rapid therapy tuning, improving the wellness of PKU patients.

KEYWORDS: phenylalanine sensing, gold-nanostructures, phenylketonuria, point-of-care, enzymatic reaction
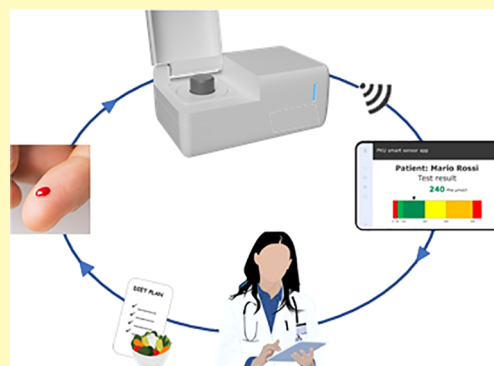
Self-monitoring of biochemical markers is gaining traction in the clinical field to help enable better the personalized healthcare and telehealth.[1,2] Recent efforts have been focused on miniaturized sensors that can recognize biomarkers, through optical or electrochemical analyses, on the surface skin (wearable devices),[3−5] inside the body (implantable sensors),[6] and on human fluids such as blood, saliva, and urine (portable sensors).[7,8] Biosensors for biomarker self-monitoring are achieved by combining key enabling technologies such as nanotechnology, nanomaterials, molecular biology, microfluidics, Internet-of-things, and artificial intelligence.[9−15] Their application has been proven effective in medical research and motivational for patients with chronic diseases. In this scenario, our team has developed innovative strategies for phenylalanine (Phe) monitoring in phenylketonuric patients based on colorimetric assay.[16,17] Phenylketonuria (PKU) is an inherited metabolic disease belonging to the disorder of amino-acid metabolism. In PKU patients, mutations in the gene *PAH* give rise to an absent or greatly reduced activity of the corresponding enzyme PAH (phenylalanine hydroxylase), which converts phenylalanine to tyrosine (Tyr). PAH is a BH4-dependent enzyme; therefore, some PKU forms may be caused by deficiencies in one of the enzymes involved in the synthesis or regeneration of the BH4 cofactor.[18,19] Since Phe cannot be converted to Tyr, it accumulates in body fluids and

becomes toxic. The typical clinical symptoms of PKU patients include intellectual disability, microcephaly, and other neurological corollaries such as epilepsy or movement disorders (Figure 1A).[20] The putative mechanisms driving the central nervous system alterations is still unclear; however, literature data converge on some key points. Phenylalanine crosses the blood brain barrier (BBB) using the L-type amino acid transporter (LAT1) in competition with the other large neutral amino acids (LNAA). Due to the high affinity of LAT1 for Phe, when its blood concentration is elevated, it preferentially crosses the BBB at the expense of other LNAA, resulting in high cerebral concentrations of Phe and low cerebral concentrations of other LNAA. This combination leads to patho-mechanisms involving metabolic alterations such as oxidative stress, neurotransmitter synthesis, and protein, lipid, and energy metabolism.[21] Therefore, in order to prevent or mitigate these clinical findings, patients with PKU are forced to follow a rigorous low-Phe diet for life. In fact, despite over time
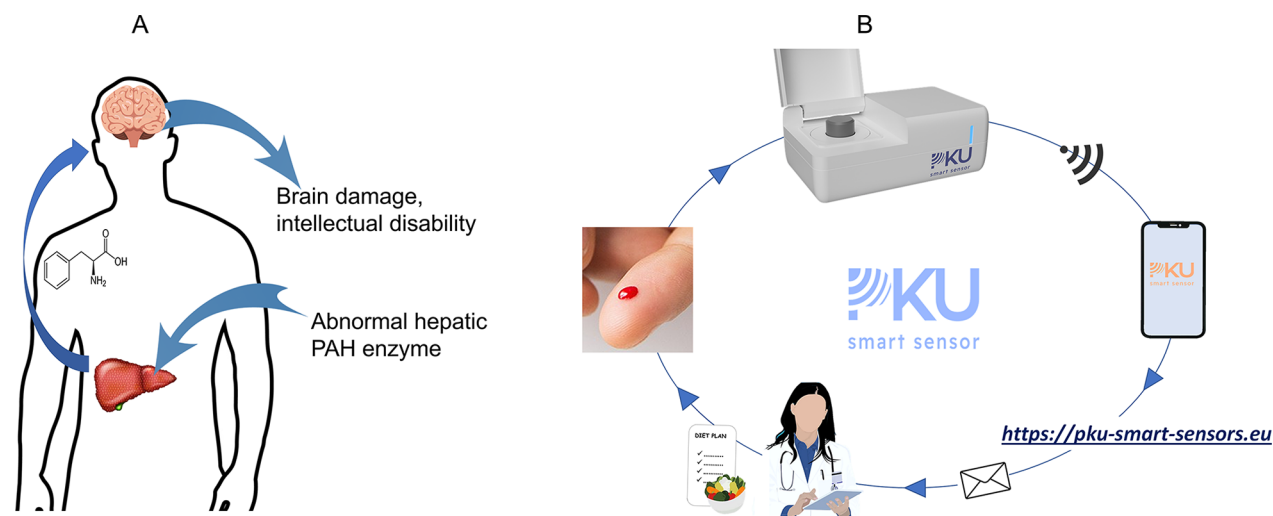
Figure 1. Schematics of the integrated "PKU smart sensor" system. (A) PKU disease features; (B) schematic of the "PKU smart sensor" platform that enables Phe monitoring from finger-prick to clinicians' feedback for daily therapy tuning.

several attempts at treatments have been done, the diet therapy turns out to be the most efficient therapy for patients with PKU. Further, they must take amino acid supplements as well as low-protein versions of common foods, specifically created for them, in order to ensure they are getting all the nutrients required to guarantee normal growth and good health.[22,23] The compliance with a strict diet remains a very complex issue for people with PKU, especially during adolescence or young adulthood.[24−26] The only way they can track their progress with the diet is by monitoring blood phenylalanine concentrations. The regular monitoring allows to evaluate the impact of dietary treatment as well as to modulate it, in order to avoid incurring neurological damages. The frequency of monitoring depends on several factors such as age, aptitude to respond to the diet/drug therapy, or particular physiological conditions such as pregnancy.[27,28] Currently, the best choice for Phe concentration monitoring is dried blood spot (DBS) testing. It consists of a drop of blood collected on a special filter paper, which, once dried, can be sent to a clinical metabolic center for analysis. The measurements are carried out by tandem mass spectrometry, which provides analysis for phenylalanine and its ratio with tyrosine.[29−31] However, this monitoring methodology is quite long for data return (4−5 days), and patients do not have immediate feedback on their diet compliance. In this regard, a point-of-care system for phenylalanine monitoring, similar to a blood glucose monitor for diabetes, would supply quick results and feedback, assisting the diet management day by day.

During the last years, different enzymatic and nonenzymatic approaches for Phe recognition have been reported in the literature. Most of them are based on colorimetric[32−34] and electric detection,[35−37] and some of these were successfully integrated into miniaturized devices,[33,38] including wearable sensors.[39] Despite the declared good analytical performances, they appear difficult to be developed in a fully integrated platform for commercial purposes, due to different constraints such as high cost analysis, laborious procedures, and limited usability. Other ones need to be tested with the samples from PKU patients and compared with the results obtained with the standard methods.[39] Against this background, here, we describe the "PKU smart sensor" platform, a portable, fully integrated, and wireless point-of-care system for the self-

monitoring of Phe concentration in PKU patients. The system was designed in a sample-in-answer-out format from the blood finger-prick to the daily therapy plan management (Figure 1B). To accomplish this, multifaceted challenges in the area of enzymatic biosensing strategy, innovative nanostructured materials, system integration (sensor, electronics, and mobile application), and Internet-of-things technology are addressed through a holistic approach described below.

■ EXPERIMENTAL SECTION

Materials and reagents. All chemicals included L-phenylalanine (Phe) 98% (M.W. = 165.19 g mol^{-1}), phenylalanine dehydrogenase from Sporosarcina (PDH) (>6.0 U/mg), beta nicotinamide adenine dinucleotide hydrate NAD$^+$ (M.W. = 663.43 g mol^{-1}), cetyltrimethylammonium bromide (CTAB), tetrachloroauric(III) acid trihydrate, agarose (M.W. = 306.26 g mol^{-1}), monosodium phosphate, Tris−EDTA, and 2-morpholinoethanesulfonic acid monohydrate (MES) were purchased from Sigma-Aldrich. Deionized water (MeQ) was used for all experiments. The GR separation membrane (thickness of 300 ± 20 μm, from PALL, grade GR) was used for plasma filtration. The MF1 glass fiber membrane was used as an optical contrast membrane (Whatman; thickness, 367 μm; wicking rate, 29.7 s/cm; water absorption, 39.4 mg/cm^{-3}). An L-amino acid spectrophotometric commercial quantitation kit (cod ACMAK002 KT) was used.

Preparation of the Optical Contrast Membrane. An aliquot of colorimetric reagents composed by 62.2 μL of AuCl$_4^-$/CTAB and 18.7 μL of AuNP seeds was deposited on a nitrocellulose membrane (MF1; diameter, 8 mm) and dried at 70 °C for 30 min in an incubator. The membrane was mounted at the bottom of the holder B. The reagent mixture HAuCl$_4$/CTAB was prepared by dissolving 135 mg of CTAB in a volume of 10 mL of deionized milli-Q water, under stirring. After dissolution, an aliquot (180 μL) of HAuCl$_4$ (5 × 10^{-2} M) was added, and an orange solution was obtained. The AuNP seeds were prepared by dissolving an aliquot of 75 μL of HAuCl$_4$ (5 × 10^{-2} M) in 37.5 mL of deionized milli-Q water; after 20 min of stirring at a temperature of 70 ± 5 °C, an aliquot of sodium citrate was added (sodium citrate stock solution of 28.5 mg/2.5 mL). After 1 h of reaction, the red-purple dispersion of AuNPs was centrifuged at 13,000 rpm for 5 min, and the precipitated AuNPs were purified by washing with deionized milli-Q-water and centrifugation.

Preparation of the Thermoresponsive Membrane. 0.4 g of agarose was dissolved in 100 mL of deionized milli-Q water under continuous stirring at a temperature of 80 ± 5 °C for 20 min. A volume of 150 μL of 0.4% agarose solution was dispensed onto the

surface of an optical contrast membrane. A solid thermoresponsive membrane was obtained after cooling at room temperature.

Preparation of the Enzymatic Layer. At the surface of the thermoresponsive membrane, the enzymatic reagent layer was deposited (0.3 mol of NAD+ and 0.035 UI of PHD) by drop-casting and dried at room temperature.

Human Subject Recruitment. The sample collection was made up of 16 withdrawals of whole blood, obtained from PKU and BH4 patients and healthy controls. The recruitment of patients was designed as follows: 1 BH4-deficit (female, 14 years old), 13 PKU (6 female and 7 male, ranging from 2 to 41 years old), and 2 healthy controls (1 male, 48 years old, and 1 female, 27 years old). The enrolled patients were clinically followed up in our Referral Center for Inherited Metabolic Disorders, located at the Polyclinic of Catania, Italy. Informed consent was obtained from all subjects involved in the study, including minors whose informed consent was signed by parents (resolution no. 27819——July 10, 2020 of Ethic Committee—Polyclinic of Catania and resolution no. 1327—July 20, 2020 of Polyclinic of Catania). During a follow-up visit, each patient underwent drawing of blood. Immediately, a few microliters of each whole blood sample was spotted on a Whatman 903 filter paper (Eastern Business Forms, Greenville, SC, USA), getting a dried blood spot (DBS). Each DBS was dried away from direct sunlight or heat sources, and after about 4 h, it was ready for mass spectrometry measurements. All samples were collected after 3 h of fasting.

Genetic Analysis of Human Sample. All real samples collected by volunteer patients were molecularly confirmed. Genetic analyses were performed by the Molecular and Cell Biology Laboratory, Pediatric Neurology Unit and Laboratories, Meyer Children's Hospital, Florence, Italy. Measurements were carried out on a MiniSeq system (Illumina, San Diego, CA, USA) with the paired-end 150 bp protocol. The sequencing was preceded by selective enrichment using an amplicon-based strategy (Ampliseq for Illumina, San Diego, CA, USA). The total coverage of the coding gene was ensured by Sanger sequencing. Data analysis was performed on the platform BaseSpace Sequence Hub with DNA amplicon (v2.1.0). Variant annotation was performed using the ANNOVAR tool.

Tandem Mass Analysis for Biosensor Validation. Measurements were carried out by the Neobase2 nonderivatized MSMS kit (Wallac Oy, Turku, Finland), according to the manufacturer's instructions. In brief, using an automatic puncher (PerkinElmer Panthera Puncher), filter paper disks (3.2 mm in diameter) were punched out from the DBS into the wells of a microplate, and 125 μL of a working solution was added into each well. The plate was shaken in the incubator/shaker (TriNest incubator, Wallac Oy, Turku, Finland) at 30 °C for 30 min at a speed of 750 rpm, and then 100 μL from the content of each well was transferred to another microplate to avoid the presence of the paper disk during the injection inside the mass spectrometer. The electrospray ionization-tandem mass spectrometry (ESI-MS/MS) analyses were performed on a 210 MD QSight spectrometer (PerkinElmer, Waltham, MA, USA) equipped with a triple quadrupole. The analysis was performed in flow injection mode using a QSight HC autosampler MD (PerkinElmer, Waltham, MA, USA) and a QSight binary pump (PerkinElmer, Waltham, MA, USA); the volume of injection was 10 μL, and the flow rate was 0.02 mL/min. The MS parameters were set up as follows: capillary voltage, 5 kV; source temperature, 175 °C, drying gas, 105 L/h; and nebulizer gas, 130 L/h. The analytical measurements were performed in multiple reaction monitoring modes (MRMs), using stable isotope internal standards for quantitative analysis.

Biosensor Operation. From a freshly finger-pricked blood drop, a volume of 20 μL was deposited on the filtration membrane. After 3 min of filtration, the module was removed, and an aliquot of sodium buffer phosphate at pH 8.5 (110 μL, 10 mM) was aliquoted at the surface. Both liquid handlings were performed through customized micropipettes. The biosensor was then closed by a lid to avoid evaporation, and the analysis started. The platform performed optical reading at time zero (S_{zero}) and every 10 s ($S_{n.sec.}$) during the thermal protocol (37 °C for 30 min and 70 °C for 50 min) and at the end of the analysis (S_{END}). Each point (S_{ZERO}, $S_{n.sec.}$ and S_{end}) was the average

of 25 measurements. The final response was calculated as the difference between S_{END} and S_{zero} (Signal = S_{END} − S_{ZERO}). This signal value was then converted to Phe concentration (μM) through the calibration line ($Y = 0.181X + 266.0$; $R^2 = 0.997$) reported in Figure 5A ($\sigma_{slope} = 0.004$ and $\sigma_{background} = 2.58$). The final response in terms of Phe concentration was displayed together with the Phe range in the mobile app.

Calibration Line Preparation. The calibration line was prepared using Phe standard aqueous solutions in different concentrations (0, 50, 200, 500, 1000, and 2000 μM). Each solution was tested with a PKU smart sensor platform, and the signal value was related to the Phe concentration. For comparison, the Phe concentration was measured by a commercial amino acid reagent kit.

■ RESULTS AND DISCUSSION

PKU Smart Sensor System. The PKU smart sensor system composed of a disposable biosensor, custom-reusable electronic system, mobile app, and cloud computing was designed, fabricated, developed, and tested (Figure 1B). Sample treatment, molecular-level enzymatic recognition, and transduction optical signals integrated on the biosensor are gathered by the electronic system, and the results are wirelessly transmitted to the wearer's mobile application (mob app) for user visualization. The data storage and the direct connection with clinicians are managed by a customized cloud computing system (Figure SI5, Supporting Information). The proposed PKU smart sensor platform was recently patented.[40] The disposable biosensor depicted in Figure 1B integrates all the required steps for Phe quantification including blood filtration, enzymatic Phe recognition, and optical transduction. In particular. the filtration module composed by a blood filter membrane embedded on holder A was designed for plasma filtration. The sensing module (holder B) composed by an optical transparent polycarbonate support integrates: (i) the optical contrast membrane properly designed for optical measurement and for colorimetric reagents on board, (ii) the thermoresponsive membrane composed by agarose-0.4%, and (iii) an enzymatic layer containing all the enzymatic reagents predeposited at the solid polymer surface. The optical readout is performed by reflectance measurements at the optical contrast membrane surface (Figure 2C). The assay result is displayed on the smartphone (PC or tablet) main page display.
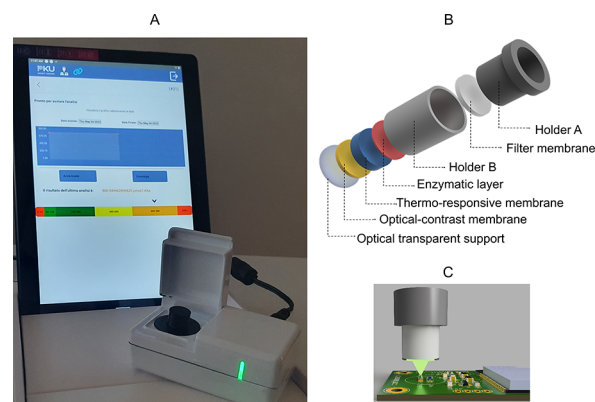

Figure 2. Schematics and images of "PKU smart sensor" system and biosensors. (A) PKU smart sensor platform photograph; (B) biosensor components for plasma filtration (holder A and filter membrane), Phe enzymatic recognition (holder B, enzymatic layer), and colorimetric transduction (thermoresponsive membrane and optical contrast membrane); and (C) optical readout by reflectance measurement.

According to the European guidelines on phenylketonuria,[27,28] the PKU smart sensor response is arranged in six Phe concentration ranges, as detailed in a later section.

Integrated Biosensing Strategy. Figure 3 provides an overview of the biosensing strategy, which was designed for
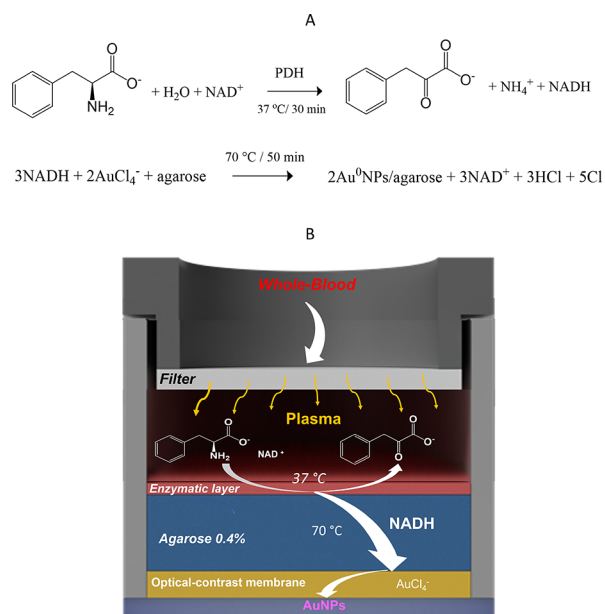

Figure 3. Biosensing strategy overview: (A) enzymatic and colorimetric transduction reactions and (B) biosensing strategy into biosensors.

functionality, full integration, sensitivity, specificity, compactness, and easy procedures. Phe detection with high sensitivity and selectivity was achieved through the careful design of the reactions schemed in Figure 3A. It is based on: (i) enzymatic conversion of phenylalanine to phenylpyruvate, assisted by the enzyme phenylalanine dehydrogenase (PDH), NAD$^+$-dependent, with the production of NADH and ammonium; this step is performed at 37 °C for 30 min; (ii) transduction reaction performed at 70 °C for 50 min, which involves the transfer of electrons from the neo-formed NADH to AuCl$_4^-$ to promote the in situ gold nanoparticle formation spectroscopically detectable by the optical measurement of the localized surface plasmon resonance (LSPR) band in the visible wavelength region (550−900 nm); and (iii) optical reflectance measurement on the membrane surface. Figure 3B depicts the integration of the sensing mechanism into the biosensor. In detail, human blood collected by finger-pricking is filtered by a polysulfonate membrane (thickness of 100 μm and diameter of 0.8 mm) on the filtration module. The filtration process yield was about 14 ± 1 μL of plasma collected from a volume of 20 μL of whole human blood. Then, the filtered plasma is directly deposited on the enzymatic layer with on-board enzymatic reagents. Here, the conversion of Phe to phenylpyruvate occurs at 37 °C. After that, few minutes of heating at 70 °C (heating rate of 8 °C min^{-1}) induces the melting of the thermoresponsive membrane, permitting the direct reaction between the neo-formed NADH and the gold precursor reagents at the optical contrast membrane surface. The optical readout is performed in real time through reflectance measurements in the wavelength range of 550−900 nm directly at the optical contrast membrane. The optical measurements, related to the quantity of NADH generated by the enzymatic reaction, can be

quantitatively related to the Phe amounts in plasma, as confirmed by the Phe dose−response calibration line in a later section.

The proposed enzymatic colorimetric strategy was spectroscopically investigated in the wavelength range of 250−1000 nm (using a standard quartz cuvette, l = 1 cm). Figure 4A

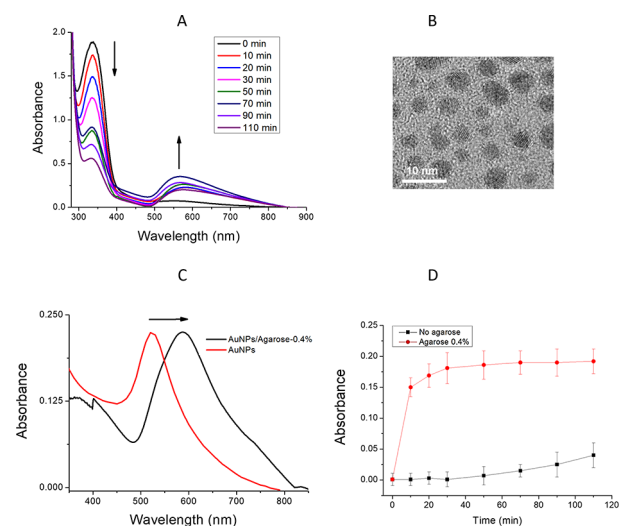**Figure 4.** Biosensing characterization: (A) optical absorption spectra changes for the enzymatic colorimetric recognition of Phe (400 μM); (B) representative TEM indentation of gold nanoparticles prepared in solution; (C) optical absorption spectra for Au nanostructures formed in the absence (red line) and in the presence (black line) of agarose-0.4%; (D) kinetics of Au nanostructure formation in the presence (red circle) and absence (black circle) of agarose-0.4%.

depicts the optical spectra changes for the enzymatic colorimetric recognition of Phe 400 μM at different reaction times. The optical absorption changes clearly indicate the disappearance of the absorption band at 340 nm related to the conversion of NADH to NAD$^+$ and the appearance of the LSPR absorption band at around 590 nm to confirm the Au nanostructure formation. The Au nanoparticle formation was confirmed by TEM investigation (Figure 4B). A diameter of 8 ± 2 nm was observed for the nanoparticles in solution. The multifunctional thermoresponsive agarose-0.4% layer was properly engineered to (i) guarantee a melting temperature above the temperature of the enzymatic reaction (37 °C) and below the temperature of the colorimetric transduction (70 °C), in order to keep the reactants separate during the enzymatic step, avoiding enzyme inhibition or nonspecificity; (ii) ensure a biocompatible solid surface on which the enzyme reagents are deposited and perform the enzyme reaction; (iii) allow an effective mixing between the products of the enzymatic reaction (NADH) and the reagents for optical transduction upon the melting process (70 °C for 3 min); (iv) form gold nanostructures characterized by the LSPR band at wavelengths greater than 560 nm, eliminating the interference with the biological sample; and (v) increase the gold formation kinetics, reducing the time of analysis. Figure 4C illustrates the optical absorption spectra of the gold nanostructures with and without agarose-0.4%. A sharp LSPR band at around 532 nm was observed for the gold nanostructures formed in the absence of agarose, whereas a broad and red-shifted LSPR band at around 590 nm was evident in the presence of agarose, as expected for the aggregation of gold nanostructures in
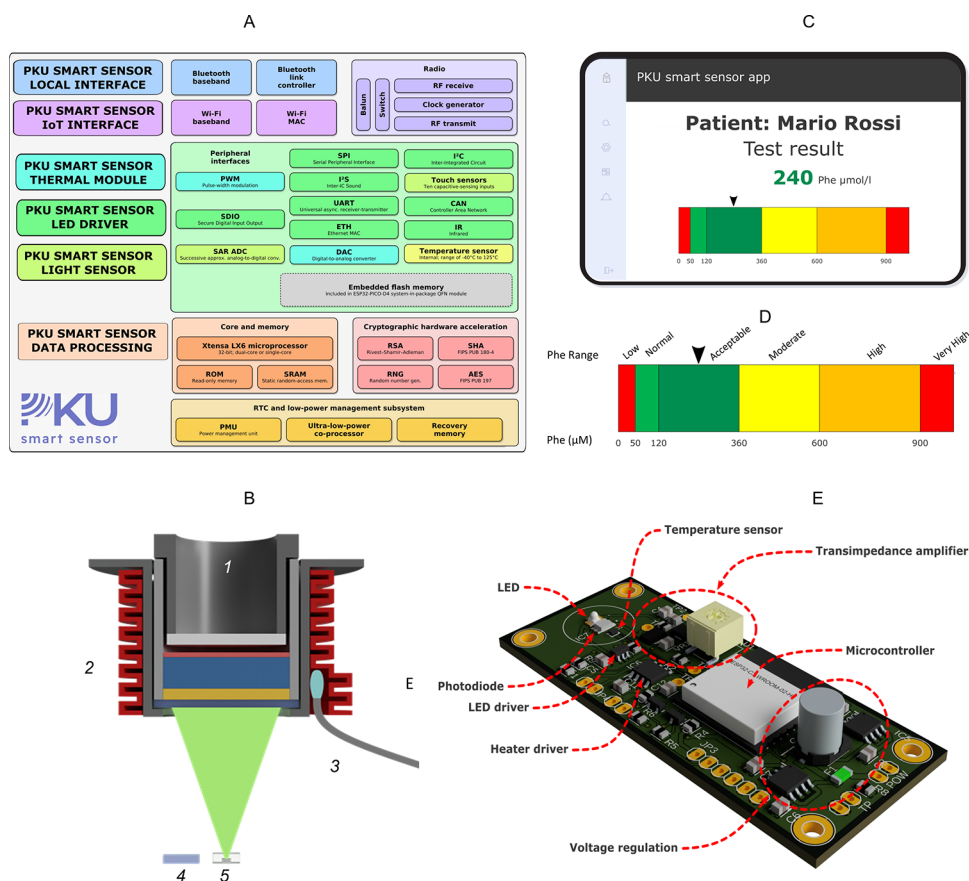
Figure 5. Electronic system of the PKU smart sensor: (A) Block diagram of the electronic system of the "PKU smart sensor": the thermal and optical units are included in the thermal module, LED driver, and light sensor components. Data processing, local interfaces, and IoT interface modules are included. (B) Architecture of the thermal and optical modules: (1) biosensor, (2) heater, (3) temperature sensor, (4) photodiode, and (5) LED source. (C) Customized mobile app for Phe tracking. (D) Phe range according to guidelines. (E) Major component labels on electronics.

polymeric media.[41] Moreover, our experiments indicate that the agarose-0.4% layer improves the efficiency of gold nanostructure formation due to the capping effect of agarose to stabilize the gold nanostructures.[42] Figure 4D reports the kinetics for the enzymatic recognition of Phe in the absence (black squares) and presence (red circles) of agarose. The graph reports the absorbance values measured at both maximum peaks (530 and 590 nm) over time. The data clearly indicate that with agarose, after about 15−20 min of reaction, the absorbance reaches the plateau value (A_{590nm} = 0.18), whereas in the absence of agarose, a lower reaction rate occurs. For comparison, the enzymatic colorimetric strategy in the absence of agarose was spectroscopically investigated, and the optical absorption spectra change showed the appearance of the LSPR at 532 nm at different reaction times for the recognition of 200 μM Phe (Figure SI6, Supporting Information).

Design and Overview of the Biosensor, Reader, and Wireless Interface System. The disposable and low-cost biosensor was fabricated using a cost-effective and reproducible 3D-printing machine using FDM technology to print a three-dimensional optimized design from a stock PETG filament material. The biosensor consists of two cylindrical modules designed for plasma filtration and Phe sensing recognition. The plasma filtration module housed inside the sensing module was properly designed to collect a volume of about 20 μL of human blood. It is equipped with a polysulfonate membrane for quantitative plasma separation. As depicted in Figure 2B, the

multilayered sensing module is composed by an optically transparent support, a nitrocellulose optical contrast membrane containing the chemicals for colorimetric transduction, thermoresponsive membrane composed by agarose (0.4% w/w), and an enzymatic layer containing PDH and a cofactor (NAD$^+$) for the Phe sensing process. The electronic reader system is composed of optical and thermal modules, a microcontroller, and power supply (Figure 5A). The disposable biosensor is housed with a proper geometry on an electronic system for effective and reproducible heating and optical reading processes, as schemed in Figure 5B. More in detail, the optical module is composed by two elements, a LED driven with a current driver for the sample light excitation and a photodiode coupled with a transimpedance amplifier to measure the reflected light from the sample. The thermal module is composed of a motor driver attached to a heating resistor wrapped around the biosensor and a voltage divider circuit attached to an NTC thermistor positioned between the sample and the heating resistor (Figure 5C). The microcontroller module is composed by an ESP32 microcontroller to manage both the communication with the external control app via Bluetooth and the interactions with the other modules via the IC2 interface and its native ADC converter. In addition, the microcontroller manages the following tasks: (i) temperature control of the sample through PID driving of the heating resistor using the NTC thermistor as the temperature feedback, (ii) acquisition routine: turning ON the LED, measurement of the reflection data from the photodiode, and
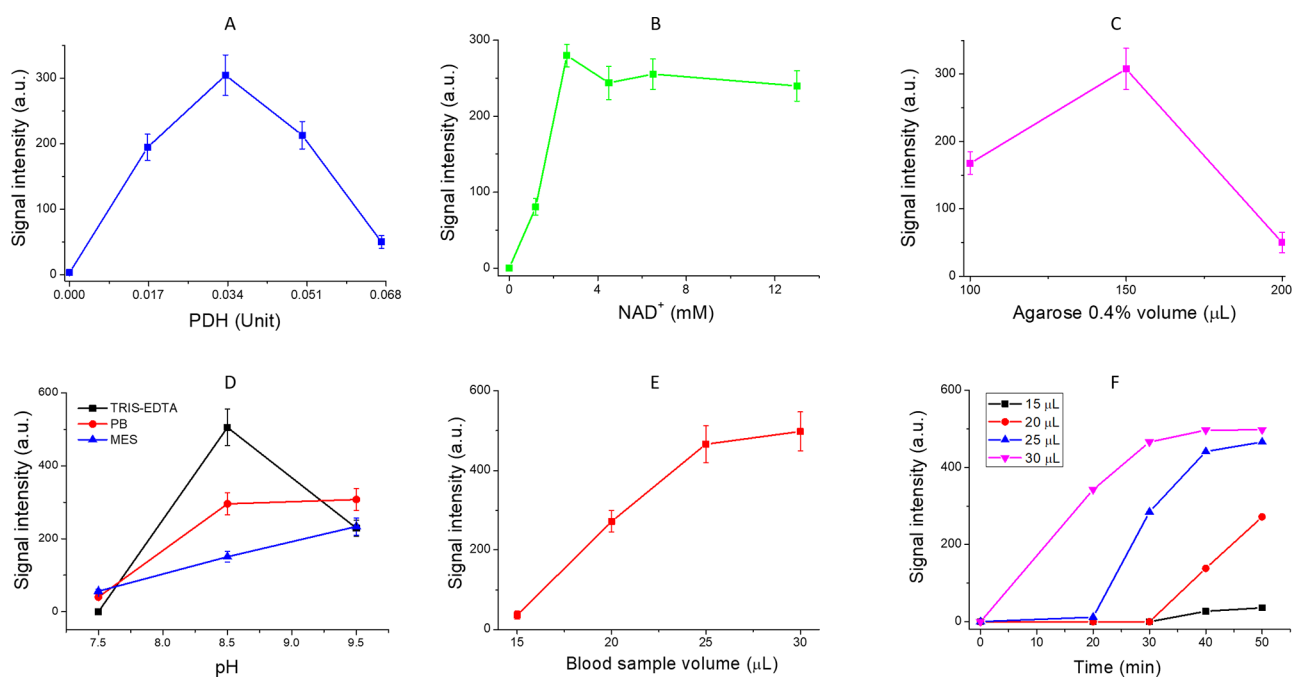
Figure 6. Biosensing procedure optimization: biosensor responses for (A) different PDH enzyme amounts (0, 0.016, 0.035, 0.05, and 0.067 U); (B) different NAD$^+$ cofactor concentrations (0, 1.2, 2.6, 4.5, 6.5, and 13 mM), (C) different thermoresponsive agarose-0.4% volumes (100, 150, and 200 μL), (D) different pH values (7.5, 8.5, and 9.5 pH units) and buffer compositions (1 mM Tris−EDTA, 10 mM phosphate buffer, and 1× MES); (E) biosensor signals for different whole blood volumes (15, 20, 25, and 30 μL) after 50 min of reaction; and (F) real-time biosensor response for different whole blood volumes (15, 20, 25, and 30 μL).

turning OFF the LED, (iii) experiment routine: handling of all the experimental parameters like duration and temperatures, (iv) data analysis: all the data from the experiments are processed on board and sent to the external control app, (v) power supply module: the power supply module handles all the supply needed for the other components on the reader; it converts the external supply voltage of 12 V to 5 and 3.3 V. Mobile application was developed with standard approaches. The mobile application can wirelessly communicate with the reader via Bluetooth to send the command to acquire, process, and visualize the Phe level. The mobile application establishes a secure Bluetooth connection. The main page shows available devices, connection status, and information about the analysis (date, time, and final response) (Figure 5C). When the measurement is prompted, the app extracts the current signal using a custom baseline correction algorithm and then converts the current to the corresponding Phe concentration. The final Phe level is displayed in the main page in a concentration scale bar (Figure 5D). In details, Phe range named "Low" is designed for Phe concentration <50 μM, "Normal" for Phe concentration ranging from 51 to 120 μM, "Acceptable" for Phe concentration ranging from 121 to 360 μM, "Moderate" for Phe concentration ranging from 361 to 600 μM, "High" for Phe concentration ranging from 601 to 900 μM, and "Very High" for Phe concentration >900 μM. The electronic board depicted in Figure 5E shows the practical implementation of all the previously described modules. It has been designed through an ECAD design software; the firmware that implements the microcontroller features has been written in C language and compiled with the ESP-IDF development kit. It was flashed onto the microcontroller on the board through a USB serial converter board using the ESP-IDF tools provided by Espressif. The analysis data results are transferred to a cloud for storage and clinician sharing. The Web site (https://pku-

smart-sensors.eu) connected to the clouds was developed to store, visualize, and manage all the analyses performed by the registered patients. After each analysis, an alert is promptly sent to the reference clinician to advice about the response, in order to operate an on-time diet therapy tuning.

Biosensing Optimization Procedures. The biosensing procedure was investigated and optimized through a detailed design of experiments, testing different experimental conditions in terms of buffer composition, pH, enzyme, NAD$^+$ amount, and agarose volume. All tests were performed using a standard solution of Phe (200 μM). Figure 6A depicts the biosensor responses for different PDH enzyme amounts (0, 0.016, 0.035, 0.05, and 0.067 U). Similarly, different amounts of NAD cofactor (Figure 6B) were investigated (0, 1.2, 2.6, 4.5, 6.5, and 13 mM). The results indicate that the enzyme amount of 0.035 U and a quantity of NAD cofactor above 2.6 mM ensure the maximum biosensor performance. The unusual behavior, observed for high PDH concentrations, reported in Figure 6A, is probably due to the less-efficient melting−mixing of NADH, mainly localized on top of the enzymatic layer due to the fast enzymatic reaction. This behavior is more evident on increasing the PHD amount. Figure 6C illustrates the biosensor signals obtained for different thermoresponsive agarose-0.4% aliquots (100, 150, and 200 μL). Clearly, the aliquot of volume 150 μL guarantees a greater biosensor signal. On the contrary, a higher agarose-0.4% volume (300 μL) produces a lower signal, reasonable due to the diluted sample, whereas a lower volume (100 μL) does not guarantee reagent separation during the enzymatic reaction, decreasing the biosensing performance. Finally, different pH values (7.5, 8.5, and 9.5 pH units) and different buffer compositions (Tris−EDTA, 1 mM; phosphate buffer, 10 mM; and MES, 1×) were deeply investigated. The data illustrated in Figure 6D clearly indicate that at pH 7.5 all buffers report a lower signal, whereas
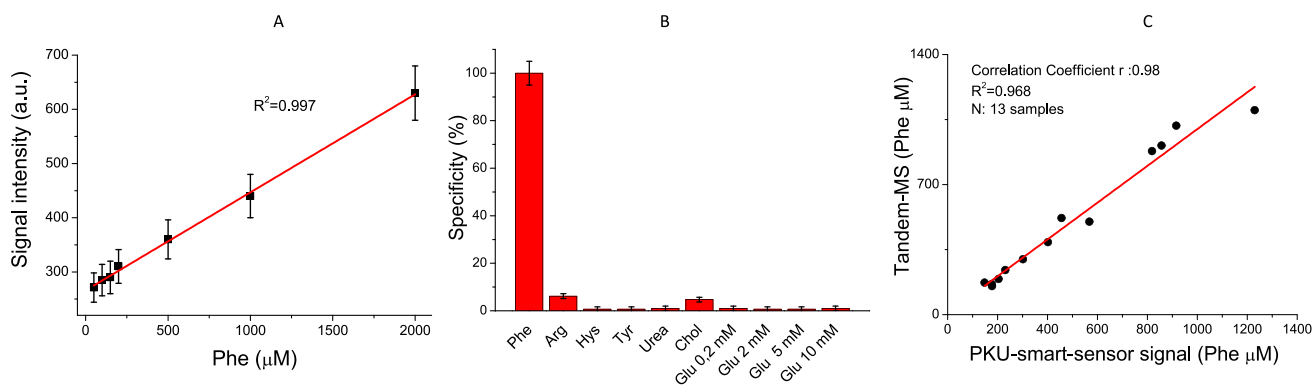
Figure 7. PKU smart sensor analytical performance. (A) Sensitivity test ($Y = 0.181X + 266.0$; $R^2 = 0.997$); (B) selectivity test; and (C) correlation between tandem MS and PKU smart sensor responses for PKU real samples.

at pH 8.5 and 9.5, the biosensing performances increase from MES, PB, to Tris. In conclusion, the optimal experimental conditions used for further experiments were: PDH, 0.035 U; NAD$^+$, 2.6 mM; agarose-0.4%, 150 μL; and 10 mM PB buffer at pH 8.5. The performance of the plasma filtration process was investigated by testing different whole blood aliquots collected by finger-prick blood sampling. In detail, different whole blood volumes (15, 20, 25, and 30 μL) were collected from PKU patients and tested using the procedure reported above. The biosensor responses illustrated in Figure 6E indicate a low signal using a blood volume of 15 μL. By increasing the blood aliquot from 20 to 25 μL, significative improvement of the biosensor signal was recorded. However, on testing a higher blood volume (30 μL), biological matrix interference occurs as indicated by the unspecific signal recorded after few minutes and as confirmed by the red-colored filtered plasma collected. Figure 6F depicts the real-time response for different whole blood volumes (15, 20, 25, and 30 μL). In summary, the best biosensor performance in terms of signal intensity and absence of interferences was reached with the blood volume of 25 μL. The Phe amount in blood samples was confirmed by tandem MS technique immediately after the collection (60 μM).

Assessment of Analytical Parameters. To evaluate the analytical performance of the PKU smart sensor, the linear response range, sensitivity, limit of detection (LoD), and selectivity were investigated. Figure 7A illustrates the linear relationship between the biosensor response and the amount of Phe. A dynamic linear range of 50−2000 μM ($Y = 0.181X + 266.0$; $R^2 = 0.997$) was observed with a sensitivity of about 0.18 au μM^{-1}. An LoD value of about 43 μM was obtained using the formula LoD = 3σ/slope (where the background standard deviation is $\sigma_{background}$ = 2.58). The capability of the assay to selectively discriminate between Phe versus other molecules was investigated. In detail, the assay was tested in the presence of arginine, histidine, tyrosine, urea, and cholesterol at a concentration of 200 μM, together with glucose at different concentrations (0.2, 2, 5, and 10 mM). The data reported in Figure 7B confirm the high specificity (∼97%) of the proposed assay for the recognition of Phe.

Phe Recognition in PKU Patients. The PKU smart sensor platform was tested using human blood samples collected from PKU and BH$_4$-deficit patients and healthy controls as references. The human participant recruitment criteria used are detailed in Experimental Section. The genetic analysis was performed for all samples to confirm the PKU and

BH$_4$-deficit diseases. The genetic analysis results reported in Table S1 confirm for patients 2, 3, 4, 5, 7, 8, 9, 10, 11, and 13 the PKU disease by typical gene mutations Similarly, the genetic analysis for patient 14 showed the typical gene mutation for BH$_4$-deficit disease. Samples 15 and 16 did not show gene mutations (negative controls). Patients 1, 6, and 12 denied the consent for current genetic analysis, but the PKU disease was previously confirmed. All samples were deeply investigated by the tandem MS technique to quantify the Phe level, as described in Experimental Section. Figure 7C depicts the experimental data correlation between the PKU smart sensor and tandem MS results. The calculated correlation coefficient (r) of 0.98 indicates a very strong linear relationship between the two methods.

More in detail, Table 1 reports the values of Phe concentration obtained with

Table 1. Phe Concentration Values Obtained with Tandem MS and PKU Smart Sensor and Relative Variance Percentage

patients	PKU smart (μM)	tandem MS (μM)	variance %
1	148	172	−13.95
2	177	164	7.93
3	178	153	16.34
4	204	192	6.25
5	231	240	−3.75
6	402	390	3.08
7	456	520	−12.31
8	568	500	13.60
9	819	880	−6.93
10	857	910	−5.82
11	1230	1100	11.82
12	916	1017	−9.93
13	302	298	1.34
14	<LoD	23.2	NA
HC1	<LoD	42	NA
HC2	<LoD	38	NA

tandem MS and PKU smart sensor for all samples investigated. The good accordance between the two methods is confirmed by the low-variance percentage values below 10% for most samples. However, all investigated PKU samples show variant percentage values (below 17%), which guarantee each concentration within the same Phe range. For completeness, a sample from BH$_4$-deficit patient was tested. The sample was collected during a poor compliance to diet therapy and

metabolic crisis. As expected, a very low Phe concentration value was obtained by tandem MS (23.2 μM), and according to these data, the PKU smart sensor response was within the Phe range "LOW". The biosensor responses for the healthy controls (HC), collected after 3 h of fasting, showed Phe concentration within the Phe range "LOW", as confirmed by tandem MS, which disclose 43 μM for HC1 and 38 μM for HC2. The real-time responses from the PKU smart sensor platform for all of the human samples investigated are reported in the Supporting Information. More results for samples with a low level of blood Phe are reported in Table S2.

Future Improvements. In order to improve the PKU smart sensor platform efficiency, additional investigations will be performed. In particular (a) to reduce the analysis time, we investigate the use of molecular additives, such as peptides, macrocycles, and so forth, for improving the thermodynamics and kinetics of the AuNP process formation; (b) artificial intelligence will be implemented to improve the doctor's feedback efficiency; (c) 2 years' long assay lifetime will be implemented, and preliminary results performed with chips stored a +5 °C indicate the least assay lifetime of 1 month (Table S3); (d) microfluidics will be integrated to improve the blood collection/filtration process; (e) proper recombinant PHD will be developed to perform a faster and room-temperature enzymatic reaction, (f) to improve the melting–mixing efficiency, molecular additives will be included in the thermoresponsive membrane; and (g) selectivity tests including a broad set of interferences will be performed.

CONCLUSIONS

In conclusion, by integrating the sample treatment process, molecular-level enzymatic recognition, and transduction optical signals from miniaturized biosensor, gathered by the electronic system wirelessly transmitted to the mobile app, we have demonstrated a powerful biosensing strategy for selective Phe detection and real-time PKU therapy tuning. This represents the first example of a fully integrated point-of-care platform tested on real samples that can be discretely used by PKU patients during their daily lives for effective therapy monitoring. Analytical performances in terms of sensitivity and specificity were investigated, obtaining a sensitivity value of about 0.18 au μM^{-1} and a LoD value of about 43 μM. An excellent specificity of about 97% was observed. All experiments with real samples were widely validated by comparison with the tandem MS technique, obtaining an excellent correlation coefficient (r) value of 0.98 to indicate a very strong linear relationship between the two methods. Although there are good platform performances, some improvements should be made, mostly focused on enhancing the enzyme stability through DNA cloning technology and integrating the finger-prick blood sampling process directly into the biosensor to further reduce the user handling. We envision that this platform could play a crucial role in the realization of the first commercial device for self-monitoring the Phe concentration in blood. Furthermore, this technology could be reconfigured to self-monitor a variety of other biomarkers toward a wide/huge range of diagnostic and personalized applications.

ASSOCIATED CONTENT

Supporting Information

The Supporting Information is available free of charge at https://pubs.acs.org/doi/10.1021/acssensors.3c01384.

PKU smart sensor platform, electronic reader, disposable and modular biosensor, mobile application, cloud computing, optical absorption spectra changes for Phe recognition 200 μM, PKU smart sensor responses for the human sample from PKU patients, human participant features, and genetic analysis (PDF).

AUTHOR INFORMATION

Corresponding Author

Salvatore Petralia — *Department of Drug and Health Sciences, University of Catania, 95125 Catania, Italy; CNR-Institute of Biomolecular Chemistry, 95126 Catania, Italy;* ⓘ orcid.org/0000-0001-5692-1130; Email: salvatore.petralia@unict.it

Authors

Maria Anna Messina — *Expanded Newborn Screening Laboratory, A.O.U Policlinico "G. Rodolico—San Marco", 95125 Catania, Italy*

Ludovica Maugeri — *Department of Drug and Health Sciences, University of Catania, 95125 Catania, Italy;* ⓘ orcid.org/0000-0003-3839-3754

Guido Spoto — *InfoBiotech srl, 90143 Palermo, Italy*

Riccardo Puccio — *InfoBiotech srl, 90143 Palermo, Italy*

Martino Ruggieri — *Expanded Newborn Screening Laboratory, A.O.U Policlinico "G. Rodolico—San Marco", 95125 Catania, Italy; Unit of Clinical Pediatrics, Department of Clinical and Experimental Medicine, University of Catania, 95125 Catania, Italy*

Complete contact information is available at:
https://pubs.acs.org/10.1021/acssensors.3c01384

Author Contributions

The manuscript was written through contributions of all authors. All authors have given approval to the final version of the manuscript. M.A.M. and L.M. contributed equally.

Notes

The authors declare no competing financial interest.

ABBREVIATIONS

Phe, phenylalanine; PHD, phenylalanine dehydrogenase; NAD, nicotinamide adenine dinucleotide; PKU, phenylketonuria; NPs, nanoparticles

REFERENCES

(1) Buskermolen, A. D.; Lin, Y. T.; van Smeden, L.; van Haaften, R. B.; Junhong, Y.; Sergelen, J.; de Jong, A. M.; Prins, M. W. J.; et al. *Nat. Commun.* **2022**, *13*, 6052 DOI: 10.1038/s41467-022-33487-3.

(2) Kalasin, S.; Surareungchai, W. *Anal. Chem.* **2023**, *95*, 1773−1784.

(3) Wang, M.; et al. *Nat. Biomed. Eng.* **2022**, *6*, 1225−1235.

(4) Tehrani, F.; et al. *Nat. Biomed. Eng.* **2022**, *6*, 1214−1224.

(5) Dong, Y.; Liu, T.; Chen, S.; Nithianandam, P.; Matar, K.; Li, J. *Adv. Funct. Mater.* **2023**, *33*, No. 2210136.

(6) Jiang, Z.; Chen, N.; Yi, Z.; et al. *Nat. Electron.* **2022**, *5*, 784−793.

(7) Wei, J.; Zhang, X.; Mugo, S. M.; Zhang, Q. *Anal. Chem.* **2022**, *94*, 12772−12780.

(8) Bashyam, A.; Frangieh, C. J.; Raigani, S.; Sogo, J.; Bronson, R. T.; Uygun, K.; Yeh, H.; Ausiello, D. A.; Cima, M. J. *Nat. Biomed. Eng.* **2021**, *5*, 240−251.

(9) Erdem, Ö.; Derin, E.; Zeibi Shirejini, S.; Sagdic, K.; Yilmaz, E. G.; Yildiz, S.; Akceoglu, G. A.; Inci, F. *Adv. Mater. Technol.* **2022**, *7*, No. 2100572.

(10) Gao, Q.; Fu, J.; Li, S.; Ming, D. Applications of Transistor-Based Biochemical Sensors. *Biosensors* **2023**, *13*, 469.

(11) Jayasekhar Babu, P.; Tirkey, A.; Mohan Rao, T. J.; Chanu, N. B.; Lalchhandama, K.; Singh, Y. D. *Anal. Biochem.* **2022**, *645*, No. 114622.

(12) Macovei, D. G.; Irimes, M. B.; Hosu, O.; Criste, C.; Yertis, M. *Anal. Bioanal. Chem.* **2023**, *415*, 1033−1063.

(13) Liu, G.; Lv, Z.; Batool, S.; Li, M.-Z.; Zhao, P.; Guo, L.; Wang, Y.; Zhou, Y.; Han, S. T. *Small* **2023**, *19*, No. 2207879, DOI: 10.1002/smll.202207879.

(14) Nasrollahpour, H.; Khalilzadeh, B.; Hasanzadeh, M.; Rahbarghazi, R.; Estrela, P.; Naseri, A.; Tasoglu, S.; Sillanpää, M. *Med. Res. Rev.* **2023**, *43*, 464−569.

(15) Maugeri, L.; Forte, G.; Messina, M. A.; Camarda, M.; Ventimiglia, G.; Consoli, G. M.; Petralia, S. *ACS Appl. Nano Mater.* **2022**, *5*, 10167−10173.

(16) Messina, M. A.; Maugeri, L.; Forte, G.; Ruggieri, M.; Petralia, S. *Front. Chem.* **2023**, *11*, No. 1164014, DOI: 10.3389/fchem.2023.1164014.

(17) Messina, M. A.; Meli, C.; Conoci, S.; Petralia, S. *Analyst* **2017**, *142*, 4629.

(18) Van Spronsen, F. J.; Blau, N.; Harding, C.; Burlina, A.; Longo, N.; Bosch, A. M. *Nat. Rev. Dis. Primers* **2021**, *7*, 36 DOI: 10.1038/s41572-021-00267-0.

(19) Himmelreich, N.; Blaub, N.; Thöny, B. *Mol. Genet. Metab.* **2021**, *133*, 123−136.

(20) Mainka, T.; et al. *Parkinsonism Relat. Disord.* **2021**, *89*, 167−175.

(21) Schuck, P. F.; Malgarin, F.; Cararo, J. H.; Cardoso, F.; Streck, E. L.; Costa Ferreira, G. *Aging Dis.* **2015**, *6*, 390−399, DOI: 10.14336/AD.2015.0827.

(22) MacDonald, A.; et al. *Orphanet J. Rare Dis.* **2020**, *15*, 171 DOI: 10.1186/s13023-020-01391-y.

(23) Rondanelli, M.; Porta, F.; Gasparri, C.; Barrile, G. C.; Cavioni, A.; Mansueto, F.; Mazzola, G.; Patelli, Z.; Peroni, G.; Pirola, M.; Razza, C.; Tartara, A.; Perna, S. *Clin. Nutr.* **2023**, *42*, 732e76.

(24) Cazzorla, C.; Bensi, G.; Biasucci, G.; Leuzzi, V.; Manti, F.; Musumeci, A.; Papadia, F.; Stoppioni, V.; Tummolo, A.; Vendemiale, M.; Polo, G.; Burlina, A. *Mol. Genet. Metab. Rep.* **2018**, *16*, 39−45.

(25) Walkowiak, D.; Bukowska-Posadzy, A.; Kałużny, L.; Ołtarzewski, M.; Staszewski, R.; Musielak, M.; Walkowiak, J. *Adv. Clin. Exp. Med.* **2019**, *28*, 1385−1391.

(26) Alptekin, I. M.; Koc, N.; Gunduz, M.; Cakiroglu, F. P. *Clin. Nutr. ESPEN* **2018**, *27*, 79−85.

(27) Van Wegberg, A. M. J. *Orphanet J. Rare Dis.* **2017**, *12*, 162 DOI: 10.1186/s13023-017-0685-2.

(28) Van Spronsen, F. J.; et al. *Lancet Diabetes Endocrinol.* **2017**, *5*, 746−756, DOI: 10.1016/S2213-8587(16)30320-5.

(29) Perko, D.; Groselj, U.; Cuk, V.; Iztok Remec, Z.; Zerjav Tansek, M.; Drole Torkar, A.; Krhin, B.; Bicek, A.; Oblak, A.; Battelino, T.; et al. *Int. J. Mol. Sci.* **2023**, *24*, 2487.

(30) Yazdanpanah, L.; Yuan, M. *Clin. Biochem.* **2022**, *101*, 35−41.

(31) Gouda, A. S.; Nazim, W. S. *Egypt. J. Med. Hum. Genet.* **2020**, *21*, 56 DOI: 10.1186/s43042-020-00100-5.

(32) Jafari, P.; Beigi, S. M.; Yousefi, F.; Aghabalazadeh, S.; Mousavizadegan, M.; Hosseini Hosseinkhani, M. S.; Ganjali, M. R. *Microchem. J.* **2021**, *163*, No. 105909, DOI: 10.1016/j.microc.2020.105909.

(33) Nakamura, K.; Yokoyama, T.; Shinozuka, N. Method for assaying l-phenylalanine and sensor. U. S. Pat. N. 6468416, 2002.

(34) DeSilva, V.; Oldham, C. D.; May, S. W.; Shunnarah, R. D. Medical device for monitoring blood phenylalanine levels. EP 1618207, 2006.

(35) (35.) Cheung, M. K.; Yang, K. A.; Nakatsuka, N.; Zhao, C.; Ye, M.; Jung, M. E.; et al. *ACS Sens.* **2019**, *4*, 3308−3317.

(36) Hasanzadeh, M.; Zargami, A.; Baghban, H. N.; Mokhtarzadeh, A.; Shadjou, N.; Mahboob, S. *Int. J. Biol. Macromol.* **2018**, *116*, 735−743.

(37) Yang, J.; Bi, Q.; Song, X.; Yuan, R.; Xiang, Y. *Sens. Actuators B Chem.* **2023**, *375*, No. 132876, DOI: 10.1016/j.snb.2022.132876.

(38) Wada, Y.; Totsune, E.; Mikami-Saito, Y.; Kikuchi, A.; Miyata, T.; Kure, S. *Mol. Genet. Metab. Rep.* **2023**, *35*, No. 100970.

(39) Parrilla, M.; Vanhooydonck, A.; Watts, R.; De Wae, K. *Biosens. Bioelectron.* **2022**, *197*, No. 113764, DOI: 10.1016/j.bios.2021.113764.

(40) Petralia, S. et al.. Metodo e dispositivo per la rilevazione di fenilalanina in campioni biologici. Patent n. IT 02022000027090, 2022

(41) Stamatelatos, A.; Tsarmpopoulou, M.; Geralis, D.; Chronis, A. G.; Karoutsos, V.; Ntemogiannis, D.; Maratos, D. M.; Grammatikopoulos, S.; Sigalas, M.; Poulopoulos, P. *Photonics* **2023**, *10*, 408 DOI: 10.3390/photonics10040408.

(42) Yadid, M.; Feiner, R.; Dvir, T. *Nano Lett.* **2019**, *19*, 2198−2206.